Author(s): Ghosh, Sukanya; Mammen, Nisha; Narasimhan, Shobhana

Title: Support work function as a descriptor and predictor for the charge and morphology of deposited Au nanoparticles

Year: 2020

Version: Published version

Please cite the original version:

Ghosh, S., Mammen, N., & Narasimhan, S. (2020). Support work function as a descriptor and predictor for the charge and morphology of deposited Au nanoparticles. Journal of Chemical Physics, 152(14), Article 144704. https://doi.org/10.1063/1.5143642

Support work function as a descriptor and predictor for the charge and morphology of deposited Au nanoparticles

Sukanya Ghosh (iD), Nisha Mammen (iD), and Shobhana Narasimhan (iD)

View Online

Export Citation

CrossMark

Support work function as a descriptor and predictor for the charge and morphology of deposited Au nanoparticles

View Online   Export Citation   CrossMark

Sukanya Ghosh,[1,2] (iD) Nisha Mammen,[1,3] (iD) and Shobhana Narasimhan[1,a] (iD)

AFFILIATIONS

[1] Theoretical Sciences Unit and School of Advanced Materials, Jawaharlal Nehru Centre for Advanced Scientific Research, Jakkur, Bangalore 560064, India
[2] Condensed Matter and Statistical Physics, Abdus Salam International Centre for Theoretical Physics, Strada Costiera 11, Trieste I-34151, Italy
[3] Department of Physics, Nanoscience Center, University of Jyväskylä, Jyväskylä 40014, Finland

[a] Author to whom correspondence should be addressed: shobhana@jncasr.ac.in. **Tel.:** +91-80-2208-2833.
Fax: +91-80-2208-2766

ABSTRACT

We show, using density functional theory calculations, that the charge, magnetic moment, and morphology of deposited Au nanoclusters can be tuned widely by doping the oxide support with aliovalent cations and anions. As model systems, we have considered Au_n (n = 1, 2, or 20) deposited on doped MgO and MgO/Mo supports. The supports have been substitutionally doped with varying concentrations θ of F, Al, N, Na, or Li. At θ = 2.78%, by varying the dopant species, we are able to tune the charge of the Au monomer between −0.84e and +0.21e, the Au dimer between −0.87e and −0.16e, and, most interestingly, Au_{20} between −3.97e and +0.49e. These ranges can be further extended by varying θ. These changes in charge are correlated with changes in adsorption and/or cluster geometry and magnetic moment. We find that the work function Φ of the bare support is a good predictor and descriptor of both the geometry and charge of the deposited Au cluster; it can, therefore, be used to quickly estimate which dopant species and concentration can result in a desired cluster morphology and charge state. This is of interest as these parameters are known to significantly impact cluster reactivity, with positively or negatively charged clusters being preferred as catalysts for different chemical reactions. It is particularly noteworthy that the Na-doped and Li-doped supports succeed in making Au_{20} positively charged, given the high electronegativity of Au.

Published under license by AIP Publishing. https://doi.org/10.1063/1.5143642

I. INTRODUCTION

The discovery that, at the nanoscale, Au need not be chemically inert is perhaps one of the most exciting discoveries to emerge from the field of nanoscience.[1] Indeed, Au nanoparticles are among the most studied systems in nanoscience because of their potential applications in not just catalysis but also plasmonics and medicine.[2–4] In order to tune their properties, one can vary their size, charge state, and morphology, as well as the support that they are placed on, with all these parameters being intimately connected.[5–9]

Studies have shown that upon changing the charge of Au nanoparticles, there is a consequent alteration in, e.g., their magnetic

properties,[10,11] plasmon frequencies,[2] and optical spectra.[12] Perhaps most interestingly, differently charged Au nanoparticles have been shown to be optimal catalysts for different chemical reactions. For example, positively charged Au clusters bind more strongly to CO,[13–17] C_2H_4,[18] and H_2[19] and are better catalysts for the oxidation of peroxidase substrate[20] and the dissociation of water.[21] In contrast, negatively charged Au nanoparticles are preferable for O_2 dissociation,[17,22,23] which is a necessary step in various oxidation reactions, including the oxidation of CO to CO_2[24–27] and NO to NO_2.[28,29] They are also better catalysts for reactions such as methanol oxidation[30] and the oxidation of organic molecules such as propylene.[31,32]

There are various ways in which the charge state of Au nanoparticles can be tuned. First, one could dope or alloy the nanoparticles themselves.[33–37] Alternatively, one could try to alter the properties of the support that the nanoparticles are deposited on. This can be done by changing the oxide chosen as the support, in particular, its acidity.[5,6,8,9,14,38–45] One can introduce defects such as F-centers (O vacancies) into the support.[5,34,46–49] One can place an ultra-thin layer of the oxide support on a metal substrate so that electrons from the latter can tunnel through the oxide to the Au nanoparticles.[5,8,50–54] One can dope the oxide support by substituting either the cations or anions aliovalently with acceptors or donors;[7,21,55–57] this is the approach we will adopt in this paper. Finally, one can place the entire system in an external electric field,[58] though the required fields are rather high.

Both calculations[7,59] and experiments[56] have shown that doping the oxide support with an electron donor can flip the geometries of the adsorbed Au clusters from three-dimensional morphologies to two-dimensional wetting conformations. This change has been interpreted in terms of a redox mechanism.[40,60] Calculations have also suggested that the change in morphology results in increased reactivity toward adsorption and dissociation of O_2.[59,61]

Our aim in this paper is to investigate how to tune the charge (and concomitantly, magnetic moment) on the deposited Au clusters by doping the MgO support. In particular, we wish to investigate what concentration of which substitutional aliovalent dopant (cationic/anionic, donor/acceptor) can produce a desired change in the charge on the Au clusters. In this paper, we study the two smallest possible cluster sizes, viz., Au monomers and Au dimers; we also investigate the larger Au_{20} cluster. Both ultrasmall and larger clusters are of current scientific interest—in fact, there is at present considerable excitement at the prospect of using single-atom catalysts.[62] It has, for example, been shown that Au monomers on ceria and iron oxide can catalyze the oxidation of CO[40,63] while also being resistant to sintering.[63] Au_{20} is of interest in that it can serve as a model for larger nanoparticles; indeed, there have been a number of previous studies on its morphology, charge state, and catalytic properties.[7,27,59,61,64,65]

We note that this manuscript is the latest in a series of papers from our group in which we have addressed related questions. First, we demonstrated that doping the MgO support with an Al donor induces the morphology of a deposited Au_{20} cluster to switch from a three-dimensional form to a two-dimensional one due to the increased electron transfer from the doped support to the Au atoms.[7] Subsequently, we showed that similar wetting transitions are also observed at other cluster sizes.[59] Next, we considered the question of which dopants might be the most effective in tuning the charge of the cluster; in this previous study,[66] we expanded the chemical space to consider four kinds of dopants: anionic acceptors, cationic acceptors, anionic donors, and cationic donors. Only a single fixed dopant concentration and only the two smallest cluster sizes (Au monomers and dimers) were considered in this earlier study.[66]

As first-principles calculations on the deposited clusters on the doped supports are computationally expensive, one would ideally like to predict the ground state geometry and/or the charge acquired by the Au clusters from the properties of the doped supports alone. In our earlier study,[66] we showed that a simple

quantity $\mathscr{D} = \Delta\chi/\Delta\mathscr{R}$ serves as a descriptor for the efficacy of aliovalent doping of oxides; here, for an anionic/cationic dopant, $\Delta\chi$ is the difference in Pauling electronegativities between the dopant and the cation/anion in the host material, and $\Delta\mathscr{R}$ is the corresponding difference in atomic sizes. Descriptors are quantities that, while being relatively cheap to compute, correlate well with a property of interest.[67–70] Typically, descriptors are assembled out of a combination of one or more microscopic properties of the system that can be computed at less cost than the property that one wishes to describe; they can be used to rapidly shortlist candidate systems that might merit further computational or experimental investigation.

While our previously introduced descriptor $\mathscr{D}$ allows one to compare (at almost zero computational cost) the efficacy of different elements as dopants, one cannot use it to compare the efficacy of different dopant concentrations. We now look for a descriptor that allows us to also examine the effects of varying dopant concentration θ, albeit at a slightly greater computational cost than is required to compute $\mathscr{D}$. We will show below that the work function Φ of the doped support is such a descriptor, correlating strongly with the charge state as well as the adsorption geometry and morphology of the adsorbed Au clusters.

II. SYSTEMS STUDIED

In this paper, we study the charge state and adsorption of Au_n clusters, where n = 1, 2 or 20, placed on supports consisting of undoped or doped MgO(001), sometimes further supported on a Mo(001) substrate.

We dope the MgO(001) support with acceptor- and donor-type impurity atoms. The impurities can be either cationic or anionic, i.e., they can replace either Mg or O atoms in MgO. The obvious candidates for acceptors/donors are the elements situated immediately to the left/right of Mg and O in the Periodic Table. Thus, one can consider Na and N as acceptor-type impurities, while, similarly, Al and F are obvious donor-type impurities. However, in a previous paper,[66] we found, using a descriptor-based analysis, that Li (which is situated immediately to the northwest of Mg in the Periodic Table) serves as a better acceptor-type impurity in MgO than either N or Na. Accordingly, in this paper, we place Au clusters on MgO supports that have been doped with either N (anionic acceptor), Na or Li (cationic acceptors), F (anionic donor), or Al (cationic donor).

Previous studies have shown that the charge of the supported Au clusters can be further tuned by placing them on an ultrathin oxide layer that is deposited on a metal support.[5,8,50–54] To investigate the effects of this in combination with the doping of the oxide support on tuning the charge state of the deposited nanoclusters, we have also considered cases where a four-layer slab of MgO(001) is placed on Mo(001).

To consider cation-doping of the support, one, two, or three out of 36 Mg atoms in a (3 × 3) supercell are substituted by Na, Li, or Al atoms; similarly, for anion-doping, one, two, or three out of 36 O atoms are substituted by N or F atoms. These correspond to doping concentrations θ of 2.78%, 5.55%, and 8.33%, respectively. We note that these are rather high doping concentrations that are used to extract trends at a relatively low computational cost; in a typical experiment, smaller doping concentrations may

be expected to be used. The Au monomer and dimer are placed on this (3 × 3) supercell of the support. For calculations on the Au_{20} cluster, a larger (6 × 6) supercell is used. To achieve a dopant concentration of 2.78% in this larger supercell, 4 out of 144 Mg or O atoms are substituted by dopant atoms. For reasons of computational expense, the Au_{20} systems are studied only at this single value of θ and also only in the absence of the additional Mo substrate underneath the MgO layers. All dopant atoms are placed in the third MgO layer based on energetic considerations. We note that we use a convention where both the MgO and Mo layers are numbered consecutively starting at the top of the slab and proceeding toward the bottom, i.e., MgO(I), MgO(II), ..., Mo(III), Mo(IV).

When an Au cluster is deposited on these supports, several initial geometries are considered when searching for the ground state geometry of the system. Note that we have also optimized the lateral position of the Au cluster relative to that of the dopant atom(s) in the support, though the energy differences between different lateral positions are found to be small, <0.04 eV.

III. COMPUTATIONAL DETAILS

Our calculations are performed using spin-polarized *ab initio* density functional theory (DFT) as implemented in the Quantum ESPRESSO package.[71] A plane wave basis set is used to solve the Kohn–Sham equations[72] with cutoffs of 30 Ry and 240 Ry for the wavefunctions and charge densities, respectively. Electron–ion interactions are described using ultrasoft pseudopotentials,[73] and exchange–correlation interactions are treated within the Perdew–Wang 91 (PW91) form of the generalized gradient approximation.[74]

As mentioned above, in our calculations, the Au monomer or dimer is placed on a (3 × 3) supercell of MgO(001) or MgO/Mo(001), while the Au_{20} cluster is adsorbed on a (6 × 6) supercell of MgO(001). The support is comprised of four layers of MgO and (if present) four layers of Mo. These thicknesses are found sufficient to obtain satisfactory convergence of the surface and interface energies, work function, and interlayer distances. Periodic images of the slabs are separated by ~14 Å of vacuum along the z direction (normal to the surface). The "dipole correction" is applied to eliminate the spurious electrostatic interactions between periodic images along the z direction.[75,76]

Brillouin zone sampling is performed using a 4 × 4 × 1 Monkhorst–Pack k-point mesh[77] for the (3 × 3) cell used for the Au monomers and dimers. The larger cell used for Au_{20} is sampled, in reciprocal space, only at the zone center Γ. Convergence is improved by using Marzari–Vanderbilt smearing with a width of 0.005 Ry.[78] Geometries are relaxed making use of Hellmann–Feynman forces and the BFGS algorithm[79] with a force convergence threshold of 0.001 Ry/bohr. All atoms are allowed to relax, except in the case of MgO/Mo supports, where the two bottom-most layers of Mo are kept fixed at the bulk interlayer spacing.

The work function, Φ, of the metal or oxide/metal system is defined as the difference in energy between the vacuum level and the Fermi level of the slab; this is computed by calculating the average electrostatic potential as a function of z, following the method

suggested in Refs. 80 and 81. Electronic charges on atoms and charge-transfers are calculated by partitioning the charge density by making use of its topological properties, following the procedure laid out by Bader.[82,83]

IV. RESULTS AND DISCUSSION

A. Geometries and energetics

1. Au monomer on doped MgO(001) and doped MgO(001)/Mo

We first check the energetics and adsorption geometry for an Au monomer on undoped MgO(001) and MgO(001)/Mo. We find that on undoped MgO(001), the most favored adsorption site is atop an O atom, which is lower in energy than adsorption atop an Mg atom by 0.41 eV. The Au–O bond distance is 2.28 Å. Adsorption of an Au monomer at a hollow site on undoped MgO(001) is not stable. In contrast, on undoped MgO(001)/Mo, an Au monomer prefers to adsorb at the hollow site, making bonds with the two nearest neighbor Mg atoms. This geometry is more stable than adsorption atop O by 0.44 eV. The shortest Au–Mg distance in the ground state geometry is 2.79 Å.

The adsorption energy of a supported Au_n cluster is defined as

$$E_{ads}(Au_n) = -[E(Au_n/supp) - E(supp) - E(Au_n)], \quad (1)$$

where the three terms on the right-hand side are the total energies, from DFT, of the supported Au_n cluster, the bare support, and the Au_n cluster in the gas phase, respectively. For an Au monomer on undoped MgO(001) and MgO(001)/Mo, we obtain $E_{ads}(Au)$ = 0.75 eV and 1.72 eV, respectively. These results are in good agreement with previous values in the literature.[5,8,50,51,84]

Next, we dope the MgO(001) surface with different types of dopant atoms, i.e., Li and Na as cationic acceptors, Al as a cationic donor, N as an anionic acceptor, and F as an anionic donor. The Au monomer is deposited on these doped MgO(001) surfaces.

When the dopant is an electron acceptor (either anionic N or cationic Na/Li), the Au monomer prefers to adsorb atop an O atom of MgO [see Figs. 1(c)–1(e)], as was the case for the undoped MgO support. However, when the dopant is an electron donor (either anionic F or cationic Al), the Au monomer acquires a larger negative charge (this will be discussed in greater detail further below), and it becomes more favorable for the monomer to adsorb at the hollow site on the surface [see Figs. 1(a) and 1(b)]. On comparing Figs. 1(a)–1(e), one also notices variations in the position of the Au monomer relative to those of the dopant atoms, though energy differences between different lateral configurations of the dopant atoms are found to be small. The adsorption energy (E_{ads}) of the Au monomer on doped MgO and d, the shortest distance between the Au monomer and an atom in the support, for doping concentration θ = 5.55%, are listed in the fourth and sixth columns of Table I.

We now consider what happens when an Mo substrate is placed below the four layers of MgO. Similar to the situation for the donor-doped MgO(001) supports, the Au monomer prefers to adsorb at the hollow site for donor-doped (anionic F or cationic Al) MgO(001)/Mo, and the adsorption site remains the same,
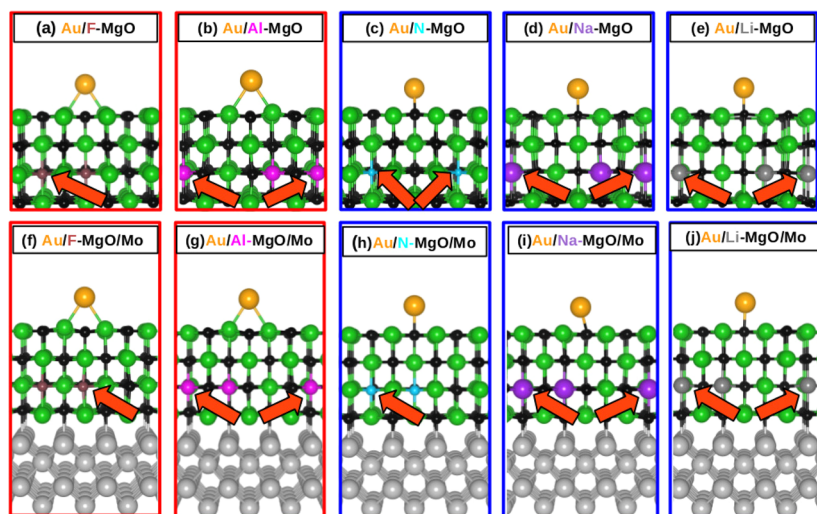
FIG. 1. Side views of ground state geometries obtained from DFT for the Au monomer on MgO(001) and MgO/Mo(001) supports that have been doped with [(a) and (f)] F, [(b) and (g)] Al, [(c) and (h)] N, [(d) and (i)] Na, and [(e) and (j)] Li. In all cases, the dopant concentration is 5.55%. Color scheme for atomic spheres: Mg, green; O, black; N, cyan; F, brown; Na, purple; Li, dark gray; Al, magenta; Mo, light gray; and Au, yellow. The orange arrows show examples of dopant atoms. Red and blue frames indicate doping by donors and acceptors, respectively. In all pictures with red frames, the Au monomer is adsorbed at a hollow site on the surface, whereas in those with blue frames, it is adsorbed atop an O atom.

irrespective of the doping concentration [see Figs. 1(f) and 1(g)]. In the case of acceptor-doped MgO(001)/Mo systems, for a doping concentration θ of 2.78%, the Au monomer adsorbs at the hollow site, bonded to the two nearest-neighbor Mg atoms. However, for the higher doping concentrations considered in this study (5.55% and 8.33%), the adsorption geometry switches to being atop O. The adsorption geometries of the Au monomer on the N, Na, and Li doped MgO(001)/Mo systems, at $\theta = 5.55\%$, are shown in Figs. 1(h)–1(j). The values of E_{ads} and d for the Au monomer on the doped MgO(001)/Mo systems at $\theta = 5.55\%$ are listed in the fifth and seventh columns of Table I. On comparing the results with and without the Mo substrate being present, we see that the biggest changes in the values of E_{ads} and d occur when the dopant is either Na or Li; the reasons for this will become apparent when we next consider the charge Q acquired by the Au monomer.

In Fig. 2(a), we have plotted our results, at $\theta = 0\%$ and 5.55%, for E_{ads} vs d. We define d as the distance between the Au monomer and its nearest neighbor atom on the substrate. We see that in the geometry atop O, where the Au monomer is bonded to a single oxygen

atom, there is a clear trend where as d decreases, E_{ads} increases. However, when instead the monomer adsorbs at the hollow site, where it bonds to two Mg atoms of the substrate, the value of d does not change appreciably upon varying the dopant element, even though E_{ads} changes.

2. Au dimer on doped MgO(001) and doped MgO(001)/Mo

On undoped MgO(001), the Au dimer prefers to adsorb atop oxygen in an upright geometry with an Au–O distance of 2.12 Å and an Au–Au distance of 2.49 Å. We find that this geometry is preferred over a flat geometry by 1.14 eV. In the ground state geometry, the adsorption energy $E_{ads}(\text{Au}_2) = 1.53$ eV.

On undoped MgO/Mo, a very similar upright geometry atop O is favored, with Au–O and Au–Au distances of 2.10 Å and 2.49 Å, respectively. The upright geometry is preferred over the flat geometry by 0.36 eV and $E_{ads}(\text{Au}_2) = 1.62$ eV in the upright geometry. All these results are in good agreement with the previous values in the literature.[5,8,50,51,84]

TABLE I. Results from DFT for geometry, energetics, and charge transfer for the Au monomer adsorbed on doped MgO(001) and MgO(001)/Mo at doping concentration $\theta = 5.55\%$. The columns list the results for the favored adsorption site: $E_{ads}(\text{Au})$, adsorption energy of Au; d, shortest distance between the Au monomer and an atom in the support; $Q(\text{Au})$, charge of the Au monomer; and $m(\text{Au})$, magnetic moment of the Au monomer.

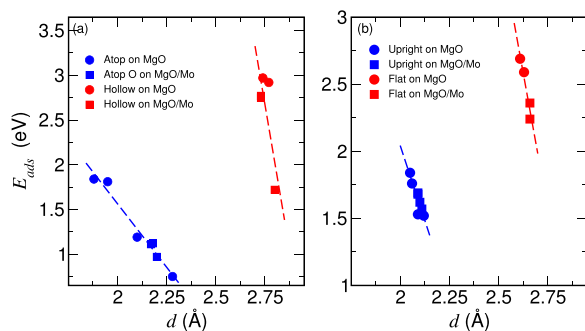| Dopant X	Adsorption site		E_{ads} (eV)		d (Å)		$Q(\text{Au})$ (e)		$m(\text{Au})(\mu_B)$	
	MgO	MgO/Mo	MgO	MgO/Mo	MgO	MgO/Mo	MgO	MgO/Mo	MgO	MgO/Mo
. . .	Atop O	Hollow	0.75	1.72	2.15	2.80	−0.27	−0.83	0.74	0.02
F	Hollow	Hollow	2.92	2.75	2.77	2.73	−0.86	−0.86	0.00	0.00
Al	Hollow	Hollow	2.97	2.77	2.74	2.73	−0.87	−0.87	0.00	0.00
N	Atop O	Atop O	1.19	1.11	2.10	2.17	−0.15	−0.38	0.32	0.73
Na	Atop O	Atop O	1.81	0.97	1.95	2.20	0.13	−0.41	0.01	0.64
Li	Atop O	Atop O	1.84	1.12	1.88	2.18	0.23	−0.39	0.00	0.75

FIG. 2. Correlation between adsorption energy and geometry for (a) Au monomer and (b) Au dimer on the various supports. E_{ads} is the adsorption energy, and d is the shortest distance between the Au atom(s) and an atom in the support. Results included are for the undoped substrates and for doping concentration $\theta = 5.55\%$. Note that for both the monomer and the dimer, the results for all supports separate into two groups, depending only on the adsorption geometry.

We will now check if and how these geometries are altered when the supports are doped. Figures 3(a)–3(e) show our results for the lowest-energy geometries of the Au dimer on the various doped MgO(001) supports. As for the case of the Au monomer in Fig. 1, in all cases, we have shown the geometries corresponding to $\theta = 5.55\%$. We see from Figs. 3(c)–3(e) that the upright geometry of Au_2 atop O is retained when the dopant is an electron acceptor (either anionic N

or cationic Na/Li). In marked contrast, when the dopant is an electron donor (either anionic F or cationic Al), it instead becomes more favorable for the dimer to adsorb in a flat geometry, with the two Au atoms forming bonds to the two nearest-neighbor Mg atoms [see Figs. 3(a) and 3(b)]. We note that a similar result has previously been found for the Au dimers on Al-doped and Mo-doped MgO, and this wetting transition is also reminiscent of the change found previously in the favored structure of an Au_{20} cluster from a three-dimensional tetrahedral geometry to a two-dimensional planar geometry upon doping the MgO support with Al donors.[7,59,61] These results are in accordance with the greater negative charges acquired by the Au dimers due to the effect of doping (this will be discussed in greater detail further below). Moreover, as was the case for the adsorption of the Au monomer, on comparing the different panels of Fig. 3, one can observe variations in the position of the Au dimer relative to that of the dopant atoms, though once again, energy differences between different lateral configurations of the dopant atoms are found to be small.

We find that, in all cases, the adsorption geometries of the Au dimers remain essentially unaltered upon introducing a Mo(001) support below the MgO [see Figs. 3(f)–3(j)].

The values of E_{ads} and d for the Au dimers (at $\theta = 5.55\%$) on the doped MgO(001) and MgO(001)/Mo supports are listed in Table II. The trends in these values can be more clearly understood by examining Fig. 2(b). We see that the results clearly fall into two groups, depending on whether the support (be it MgO or MgO/O) is acceptor-doped or donor-doped. In the former case, the dimer
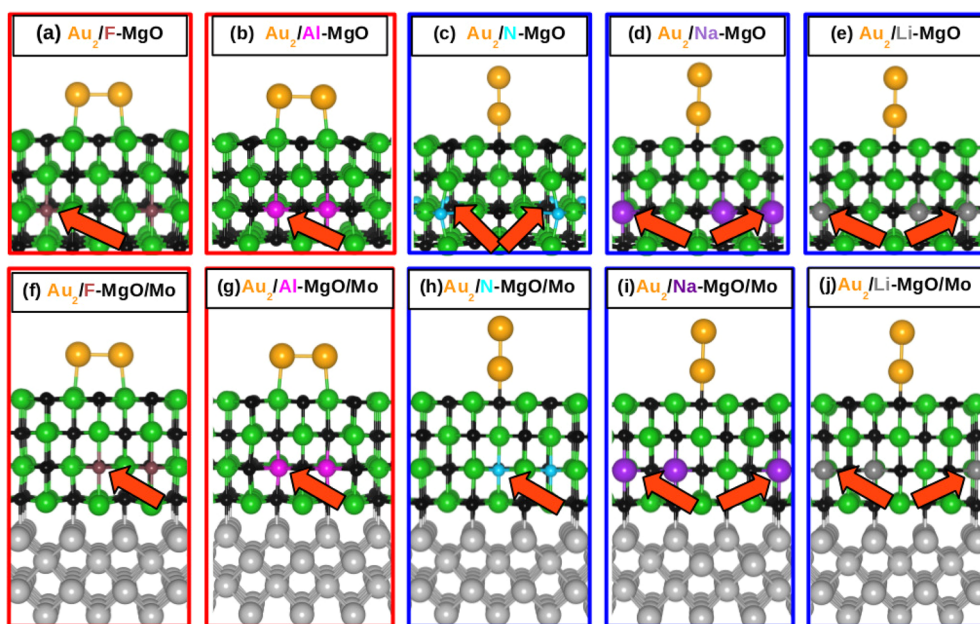

FIG. 3. Side views of the ground state geometries obtained from DFT for the Au dimer on MgO(001) and MgO/Mo(001) supports that have been doped with [(a) and (f)] F, [(b) and (g)] Al, [(c) and (h)] N, [(d) and (i)] Na, and [(e) and (j)] Li. In all cases, the dopant concentration $\theta = 5.55\%$. Color scheme for atomic spheres: Mg, green; O, black; N, cyan; F, brown; Na, purple; Li, dark gray; Al, magenta; Mo, light gray; and Au, yellow. The orange arrows show examples of dopant atoms. Red and blue frames indicate doping by donors and acceptors, respectively. Note that in all pictures with red frames, the dimer lies flat, whereas in all pictures with blue frames, it is upright, atop an O atom.

TABLE II. Results from DFT for geometry, energetics, and charge transfer for the Au dimer (Au$_2$) adsorbed on doped MgO(001) and MgO/Mo(001) at doping concentration θ = 5.55%. Results are presented for the favored adsorption site: E_{ads}(Au$_2$), adsorption energy of Au$_2$; d, shortest average distance between atoms in the Au dimer and the support; Q(Au$_2$), charge of the Au dimer; and m(Au$_2$), magnetic moment of the Au dimer. Note that the dimer is upright when it is "atop O" and lies flat when it "bonds to Mg."

Dopant X	Adsorption site		E_{ads} (eV)		d (Å)		Q(Au$_2$) (e)		m(Au$_2$) (μ_B)	
	MgO	MgO/Mo	MgO	MgO/Mo	MgO	MgO/Mo	MgO	MgO/Mo	MgO	MgO/Mo
–	Atop O	Atop O	1.53	1.62	2.12	2.10	−0.28	−0.30	0.00	0.00
F	Bonds to Mg	Bonds to Mg	2.59	2.24	2.63	2.66	−1.17	−0.97	0.59	0.77
Al	Bonds to Mg	Bonds to Mg	2.69	2.36	2.61	2.66	−1.19	−0.99	0.50	0.75
N	Atop O	Atop O	1.53	1.69	2.09	2.09	−0.25	−0.30	0.01	0.00
Na	Atop O	Atop O	1.76	1.57	2.06	2.11	−0.18	−0.28	0.19	0.00
Li	Atop O	Atop O	1.84	1.68	2.05	2.09	−0.15	−0.29	0.23	0.00

is adsorbed in an upright geometry atop O; in the latter case, the dimer is adsorbed in a flat geometry, bonded to two Mg atoms. For both groups of results, we see that though E_{ads} varies upon changing the dopant element, the effect on the adsorption geometry is relatively minor: as E_{ads} increases, there is a small reduction in d.

3. Au$_{20}$ on doped MgO(001)

In the gas phase, the most stable isomer of Au$_{20}$ is a regular tetrahedron having the length of each side = 8.02 Å. We find that this structure is favored over a planar geometry by 1.52 eV. This finding agrees well with previous experimental and theoretical results.[27,59,85] Similarly, on undoped MgO(001), a tetrahedral geometry is favored, with an adsorption energy of 1.52 eV; it is lower in energy than the lowest-energy planar morphology by 0.57 eV, again in agreement with previous results.[7,27,56,59,61,64,65] Upon adsorption on MgO, the Au$_{20}$ cluster gets slightly distorted from a perfect tetrahedron. The three edges of the tetrahedron in contact with the MgO surface have lengths of 7.98, 8.18, and 8.18 Å^3, while the remaining three sides have lengths of 8.05, 8.05, and 8.11 Å^3.

Next, we consider the adsorption of Au$_{20}$ on doped MgO for θ = 2.78%. Our results for the favored geometry in the presence of the various dopants considered are shown in Fig. 4. We find that for the three acceptor-doped systems, the cluster morphology remains tetrahedral upon introducing the dopant atoms N, Na, or Li in the support. However, for the two donor-doped systems (both anion-doped F–MgO and cation-doped Al–MgO), there is a structural transition, with the cluster now preferring to wet the support in a planar geometry. This result has been shown before for the cases of the cation-doped systems Al–MgO and Mo–CaO.[7,56,59,61] Previous authors had also shown that it was possible to induce a similar structural transition for Au$_{20}$ adsorbed on MgO by placing the ultrathin MgO film on a metal support or by placing the system in a high electric field.[27,58,64] We find that the tetrahedral geometry is favored over a planar geometry by 0.63 eV, 1.20 eV, and 1.44 eV on the N–MgO, Na–MgO, and Li–MgO supports, respectively, whereas the planar geometry is favored over the tetrahedral one by 3.94 eV and 3.81 eV on F–MgO and Al–MgO, respectively. The corresponding values of the adsorption energy E_{ads} for the ground state geometries are listed in the third column of Table III. We see that in all cases, E_{ads} is larger on doped MgO than on undoped MgO; the enhancement in E_{ads} is particularly huge in the case of the two donor-doped supports F–MgO and Al–MgO, where there is a sixfold increase in E_{ads}.

B. Charge transfer

1. Au monomer on doped MgO(001) and doped MgO(001)/Mo

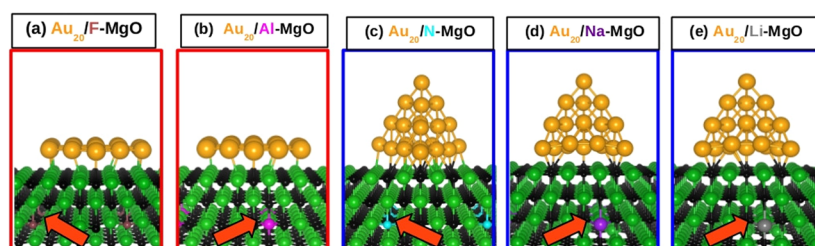The Au monomer acquires a charge of −0.27e on undoped MgO(001) and −0.83e on undoped MgO(001)/Mo. We see that the

FIG. 4. Side views of ground state geometries obtained from DFT for Au$_{20}$ on MgO(001) supports that have been doped with (a) F, (b) Al, (c) N, (d) Na, and (e) Li. In all cases, the dopant concentration θ = 2.78%. Color scheme for atomic spheres: Mg, green; O, black; N, cyan; F, brown; Na, purple; Li, dark gray; Al, magenta; and Au, yellow. The orange arrows show examples of dopant atoms. Red and blue frames indicate doping by donors and acceptors, respectively. Note that in all pictures with red frames, the Au cluster is in a planar geometry, whereas in all pictures with blue frames, it is in a tetrahedral geometry.

TABLE III. Results from DFT for geometry, energetics, charge transfer, and magnetic moment for Au_{20} adsorbed on doped MgO(001), at doping concentration $\theta = 2.78\%$. The columns contain the results for the favored adsorption geometry: E_{ads}, adsorption energy; $Q(Au_{20})$, the charge on the gold cluster; and $m(Au_{20})$, the magnetic moment of the gold cluster.

Dopant X	Stable isomer	E_{ads} (eV)	$Q(Au_{20})$ (e)	$m(Au_{20})$ (μ_B)
–	Tetrahedral	1.52	−0.91	0.00
F	Planar	9.34	−3.96	0.00
Al	Planar	9.48	−3.97	0.00
N	Tetrahedral	2.32	−0.65	0.00
Na	Tetrahedral	3.88	0.42	0.00
Li	Tetrahedral	3.95	0.49	0.00

charge transfer from the support to the Au monomer increases significantly in the presence of the Mo support, in good agreement with results from previous studies.[5,8,84]

The charge transfer is significantly modified upon doping the supports. In Fig. 5, we show again the geometries of the Au monomers placed on the doped supports, but now indicating the charge redistribution between the support and the Au atom, which occurs upon cluster deposition. In these figures, we have plotted isosurfaces of $\Delta\rho = \rho(Au_n/supp) - \rho(Au_n) - \rho(supp)$, where the three terms on the right-hand side are the electronic charge densities of the Au_n on the support, the isolated Au_n cluster, and the bare support, respectively. Note that the latter two terms are evaluated using geometries corresponding to their coordinates in the combined system. In Fig. 5, the red and blue lobes correspond to electron gain and depletion, respectively.

It is clear from Fig. 5 that in all cases, there is considerable charge transfer between the support and the Au atom; this is supported by the results obtained from the Bader analysis. Most

interestingly, we find that depending on the dopant, the Au atom can be negatively or positively charged. For F, Al, N, Na, and Li dopants in the MgO substrate, the charge on the Au monomer is $-0.86e, -0.87e, -0.15e, 0.13e$, and $0.23e$, respectively, at $\theta = 5.55\%$ (see Table I). This is in accordance with the fact that we see predominantly red lobes surrounding the Au atom in the cases where the dopant is F or Al [see Figs. 5(a) and 5(b)], smaller red lobes for N-doped MgO(001) [see Fig. 5(c)], but predominantly blue lobes in the cases where the dopants are Na and Li [see Figs. 5(d) and 5(e)]. Note that the electron acceptors N, Na, and Li have reduced (made more positive) the charge on Au relative to the value of $-0.27e$ on undoped MgO(001), whereas the electron donors F and Al have significantly increased (made more negative) the charge on Au. It is also worth noting that we find that the charge on the dopant ions themselves does not change appreciably upon deposition of the Au monomer; this is in contrast with what has been observed, e.g., for Mo dopants in CaO.[57,59]

We next wish to obtain some estimates regarding the range of positive and negative values over which the charge of the Au monomer can be tuned. Accordingly, in Fig. 6(a), we have plotted our results for how $Q(Au)$ depends on the doping concentration θ on doped MgO(001) supports. In the case of donor-doped (F and Al) MgO(001) systems, $Q(Au)$ becomes more negative than in the case of undoped MgO(001). From Fig. 6(a), we see that the magnitude of $Q(Au)$ for a given θ remains almost the same for the anionic donor F and the cationic donor Al. The charge on Au is reduced upon adsorption on acceptor-doped MgO(001). $Q(Au)$ varies approximately linearly with θ for the case of N-doping [see Fig. 6(a)], decreasing from the undoped value of $-0.27e$ to $-0.13e$. However, for the other four dopants, the value of $Q(Au)$ has already almost saturated at 2.78% and does not change appreciably on increasing θ further. Especially interestingly (given the strongly electronegative nature of Au), the cationic acceptors Na and Li make the Au monomer positively charged. The charge transfer from the
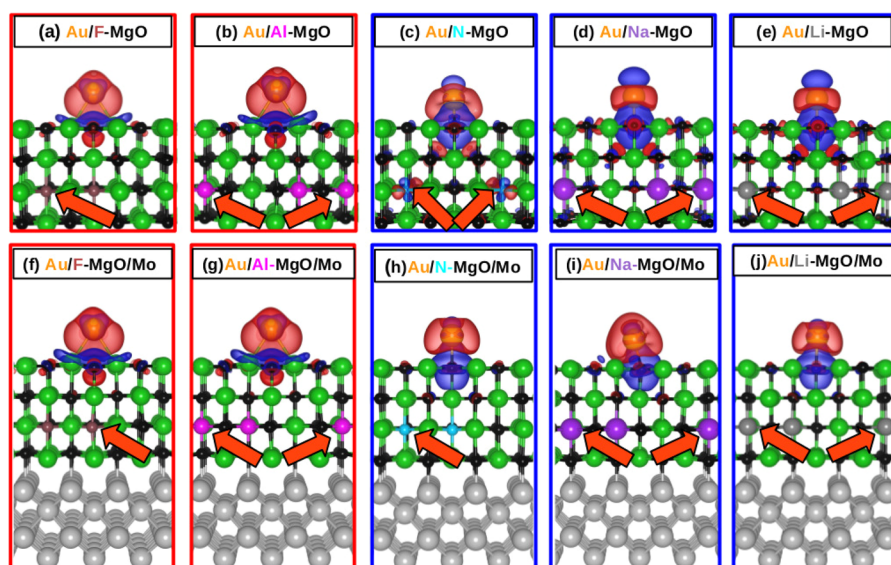

FIG. 5. Charge redistribution plots for the Au monomer on MgO(001) and MgO/Mo(001) supports that have been doped with [(a) and (f)] F, [(b) and (g)] Al, [(c) and (h)] N, [(d) and (i)] Na, and [(e) and (j)] Li. In all cases, the dopant concentration is 5.55%. Color scheme for atomic spheres: Mg, green; O, black; N, cyan; F, brown; Na, purple; Li, dark gray; Al, magenta; Mo, light gray; and Au, yellow. The orange arrows show examples of dopant atoms. Red and blue lobes show electron accumulation and depletion, respectively, drawn at isosurface values of $\pm 0.001e/bohr^3$. Red and blue frames indicate doping by donors and acceptors, respectively.
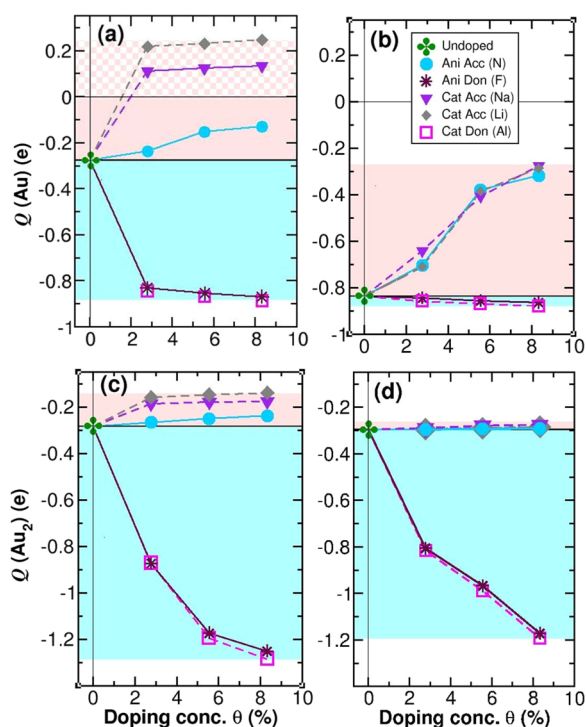
FIG. 6. Variation of $Q(Au_n)$ with doping concentration θ. Results for Au monomer on (a) doped MgO and (b) doped MgO/Mo systems and Au_2 on (c) doped MgO and (d) doped MgO/Mo systems. The cyan and pink shaded areas highlight regions where Au_n becomes more and less negatively charged, respectively, when compared to Au_n on the undoped support. The chequered pink shaded area in (a) highlights the region where the Au monomer becomes positively charged.

Au monomer to the Na-doped or Li-doped MgO increases slowly with θ. The values of $Q(Au)$ at $\theta = 8.33\%$ are $-0.87e$, $-0.88e$, $-0.13e$, $+0.14e$, and $+0.25e$ when the dopants are F, Al, N, Na, and Li, respectively. Thus, by doping the MgO(001) support, we are able to tune the charge on the Au atom over a range from $-0.88e$ to $+0.25e$. By suitably controlling the nature of the dopant and the value of θ, one should be able to achieve any desired value of charge within this range (we remark that on physical and chemical grounds, the values of θ larger than a few percent are not expected to be stable).

We also compute the magnetic moment (m) of the Au monomers using the Bader analysis where the up-spin and down-spin charges on the atoms are computed separately (see the last two columns of Table I). The magnetic moment of the Au monomer deposited on undoped MgO reduces from the value of 1 μ_B in the gas phase to 0.74 μ_B, confirming a small amount of charge transfer to the Au monomer. In the case of F-doped and Al-doped MgO, the Au monomer loses its magnetic moment, confirming the transfer of approximately one electron from the support to Au. $m(Au) = 0.32$ μ_B for N-doped MgO. For Na-doped and Li-doped MgO, $Q(Au)$ is positive and $m(Au)$ becomes close to zero, which would indicate the transfer of significant charge from the monomer to the support.

Our results may be compared with those of a previous DFT study where the Au monomer was deposited on undoped and N-doped ZrO_2.[86] The authors found that the Au monomer acquires a charge of $-0.16e$ and a magnetic moment of 0.38 μ_B on undoped ZrO_2. The charge acquired by the Au monomer can be either $+0.14e$ or $+0.29e$ on N-doped ZrO_2, depending on the position of the dopant, and in both cases, the monomer is found to be non-magnetic.

Let us now consider doped MgO supports placed on a Mo substrate. Again, when compared to the undoped case, $Q(Au)$ becomes more negative as a function of θ in the case of donor-doped MgO(001)/Mo and less negative for acceptor-doped MgO(001)/Mo (see Table I). Figure 6(b) shows the variation of the charge of the Au monomer as a function of doping concentration θ. Comparing with the results on the doped MgO supports [see Fig. 6(a)], we see that when the dopants are donors, the charge on the Au monomer remains almost the same in the presence and absence of the Mo support. Therefore, there is no advantage in placing a Mo support underneath an ultrathin MgO layer. However, when the dopants are acceptors, one sees a considerable difference in the absence and presence of the Mo support. In the presence of the Mo support, the MgO layers become more electron-rich, and then, upon deposition of Au, some of these electrons are transferred to the Au atom. Consequently, when the Mo is absent/present, the Au monomer becomes positively/negatively charged. However, this negative charge is less than that obtained on the undoped MgO support. Thus, the Mo support can be useful if it is desirable to obtain a smaller negative charge on the Au monomers. Thus, we find that $Q(Au)$ can be varied from $-0.88e$ to $-0.28e$ on different MgO(001)/Mo systems, as shown in Fig. 6(b). Note that the range of charges achievable on the doped MgO(001)/Mo supports is smaller than on the doped MgO(001) supports.

In contrast to the situation on undoped MgO, the Au monomer is very weakly magnetic on undoped MgO/Mo. The magnetic moment of the Au monomer becomes zero on F-doped and Al-doped MgO/Mo, as was also the case in the absence of the Mo substrate. The Au monomer becomes magnetic on N-doped, Na-doped, and Li-doped MgO/Mo, implying partial charge transfer from the substrate to the monomer. Note that when the dopants are Na and Li, $m(Au)$ differs in the absence and presence of the Mo support.

2. Au dimer on doped MgO(001) and doped MgO(001)/Mo

The Au dimer acquires a charge $Q(Au_2)$ of $-0.20e$ and $-0.30e$ on undoped MgO(001) and MgO/Mo(001), respectively. These values are in good agreement with previous reports in the literature.[5,8,84]

In Fig. 7, we show the charge redistribution plots for the Au dimers placed on doped MgO(001) and MgO(001)/Mo supports. As was the case for the Au monomer, one observes appreciable charge transfer between the support and the Au atoms, as indicated by the sizable red and blue lobes (corresponding to electron gain and depletion, respectively) in Fig. 7. These lobes are obviously positioned differently for the upright and flat adsorption geometries. However, the size and shape of these lobes also differ depending on the dopant species, indicating that once again, the charge gained or lost by the
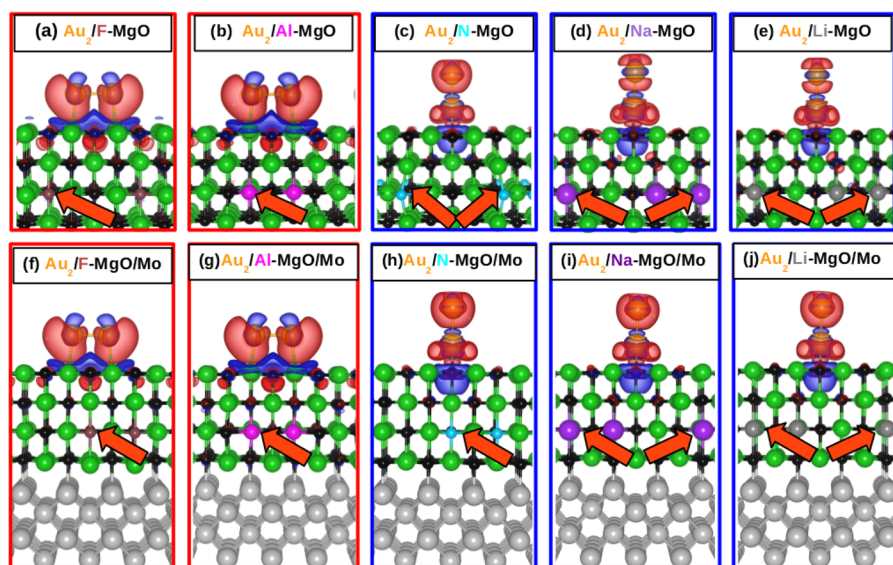
FIG. 7. Charge redistribution plots for the Au dimer on MgO(001) and MgO/Mo(001) supports that have been doped with [(a) and (f)] F, [(b) and (g)] Al, [(c) and (h)] N, [(d) and (i)] Na, and [(e) and (j)] Li. In all cases, the dopant concentration θ = 5.55%. Color scheme for atomic spheres: Mg, green; O, black; N, cyan; F, brown; Na, purple; Li, dark gray; Al, magenta; Mo, light gray; and Au, yellow. The orange arrows show the positions of the dopant atoms. Red and blue lobes show electron accumulation and depletion, respectively, drawn at isosurface values of $\pm 0.001 e/\text{bohr}^3$. Red and blue frames indicate doping by donors and acceptors, respectively.

Au dimer is not the same for the five dopants considered here. This is confirmed upon quantifying $Q(\text{Au}_2)$ using the Bader analysis (see Table II). We find that the electron donors F and Al have significantly increased (made more negative) $Q(\text{Au}_2)$, whereas the electron acceptors Na and Li have reduced it. However, in contrast to the case of the Au monomer, in no case have we succeeded in making $Q(\text{Au}_2)$ positive by doping the support. $Q(\text{Au}_2)$ does not vary much as a function of θ when adsorbed on the acceptor-doped MgO(001) supports, whereas it varies appreciably for donor-doped MgO(001). $Q(\text{Au}_2)$ varies from $-0.87e$ to $-1.25e$ for F-doped MgO and $-0.87e$ to $-1.28e$ for Al-doped MgO as θ increases from 2.78% to 8.33% [see Fig. 6(c)]. As was the case for the Au monomer, we find that for the dimer too, the effects of F-doping and Al-doping are very similar.

Next, we check how the presence of the Mo support affects the charge state of the adsorbed Au dimer. These results are presented in Figs. 6(d) and Figs. 7(f)–7(j). Qualitative trends for the dimer are similar to those discussed above for the monomer, except that the acceptor dopants are found to have no appreciable effect on the MgO/Mo supports. We find that, for the range of θ considered here, the charge of Au_2 can be tuned from $-1.19e$ to $-0.27e$ by appropriately changing the dopant and the support [see Fig. 6(d)].

The quantification of Bader charges is supported by the charge redistribution plots in Fig. 7. For example, we see smaller red lobes around the Au dimer on Na-doped and Li-doped MgO [see Figs. 7(c)–7(e)]; larger red lobes appear when the Au dimer is adsorbed on Na-doped MgO(001)/Mo and Li-doped MgO(001)/Mo [see Figs. 7(h)–7(j)].

The Au dimer is non-magnetic, both in the gas phase and when placed on undoped MgO or undoped MgO/Mo. On the doped supports, $m(\text{Au}_2)$ depends on the dopant, as listed in the last two columns of Table II. In many cases, we see that the dimer becomes magnetic, again confirming significant charge transfer between the support and the Au atoms.

3. Au_{20} on doped MgO(001)

We find that Au_{20} acquires a charge of $-0.91e$ on undoped MgO, in agreement with previous results.[7,59] This is due to charge transfer from the MgO support to the electronegative Au atoms. Both the direction and extent of this charge transfer are significantly altered upon doping the support. The values of charge $Q(\text{Au}_{20})$ on the deposited gold clusters, for θ = 2.78%, for the five dopants considered by us, are listed in Table III. We find that the donor dopants F and Al significantly increase the negative charge on Au_{20} to $-3.96e$ and $-3.97e$, respectively, whereas the acceptor dopant N reduces it to $-0.65e$. The enhancement of negative charge is interesting, as there are several chemical reactions for which it is desirable that the Au nanocatalyst have a high negative charge;[22–24,30,31] this result has also been demonstrated by previous authors.[27,59,61] The novel result that we obtain here is that two of the acceptor dopants, viz., Na and Li, are able to make Au_{20} acquire a positive charge: $+0.42e$ and $+0.49e$, respectively. As mentioned in the Introduction, there are also chemical reactions for which it is preferable for the Au nanocatalyst to be positively charged; however, given the high electronegativity of Au, coaxing Au nanoparticles into becoming charged positively has proved to be a challenging task. This is, therefore, a noteworthy result.

The values of $Q(\text{Au}_{20})$ are also supported by the charge redistribution plots [see Figs. 8(a)–8(e)]. We see predominantly red lobes, denoting electron accumulation, surrounding the Au atoms when the Au_{20} cluster is adsorbed on F-doped and Al-doped MgO(001) [see Figs. 8(a) and 8(b)]. Smaller red lobes appear on Au_{20} for N-doped MgO(001) [see Fig. 8(c)]. On the Na-doped and Li-doped supports, where the Au_{20} cluster acquires a net positive charge, we see both red and blue lobes on the Au atoms [see Figs. 8(d) and 8(e)]. The Au atoms that are in direct contact with the doped surface acquire a high positive charge, losing electrons to the substrate. The remaining Au atoms remain either neutral or acquire a small positive charge. The maximum positive charge on an Au atom
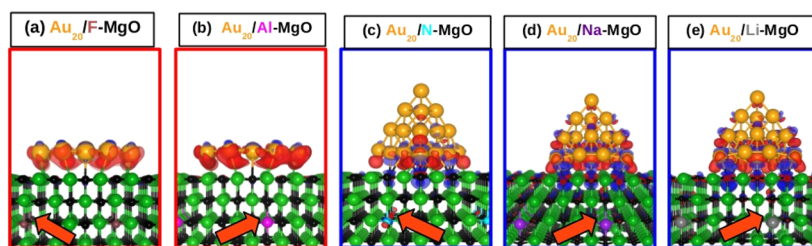
FIG. 8. Charge redistribution plots for Au_{20} on MgO(001) supports that have been doped with (a) F, (b) Al, (c) N, (d) Na, and (e) Li. In all cases, the dopant concentration $\theta = 2.78\%$. Color scheme for atomic spheres: Mg, green; O, black; N, cyan; F, brown; Na, purple; Li, dark gray; Al, magenta; Mo, light gray; and Au, yellow. The orange arrows show the positions of the dopant atoms. Red and blue lobes show electron accumulation and depletion, respectively, drawn at isosurface values of $\pm 0.002e/bohr^3$. Red and blue frames indicate doping by donors and acceptors, respectively.

in the Au_{20} cluster (having the shortest distance with the doped MgO) is $0.18e$.

Au_{20} is nonmagnetic on undoped MgO(001) and $m(Au_{20})$ remains zero on the doped MgO(001) supports.

C. Interrelationship between geometry and charge transfer

The charge acquired by the adsorbed Au cluster is intimately related with its adsorption geometry. To see this, we choose a fixed dopant concentration ($\theta = 5.55\%$) and combine the results for some of our systems (Au monomers, dimers, acceptor- and donor-dopants, and MgO and MgO/Mo supports) on a single graph. In Fig. 9, the abscissa is $Q(Au_n)$ and the ordinate is d, the shortest distance between an Au atom and an atom in the support. Red and blue symbols indicate results for the donor-doped and acceptor-doped systems, respectively, and filled dots and open triangles correspond to results on the Au monomer and Au dimer, respectively. We see that the data points cluster into two groups: one for the eight donor-doped systems and one for the twelve acceptor-doped systems. Let
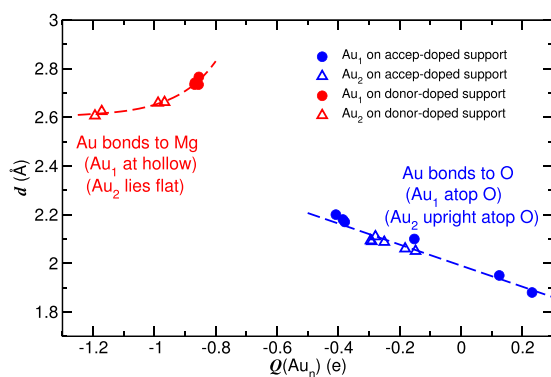
us first consider the former (red symbols in Fig. 9). In all eight cases, the Au atoms are bonded to positively charged Mg cations in the support. Therefore, as the charge on the Au atoms becomes more negative, we see that the distance d between the deposited Au cluster and the support decreases. Exactly the opposite behavior is seen for the acceptor-doped systems (blue symbols in Fig. 9). Now, the Au atoms are bonded to negatively charged O anions in the support. As a result, as the charge on the Au atoms becomes more negative, the distance d between the deposited Au cluster and the support increases. It is worth noting that the data for the monomer and dimer systems all appear to collapse onto the same two curves, depending only on whether the Au atoms are bonded to O anions or Mg cations.

D. Work function of support as a predictor of cluster morphology and charge

Earlier, we have found that we can tune both the magnitude and sign of the charge on the Au monomer, dimer, and Au_{20} by changing the support they are placed on, by varying the nature of the dopant introduced into the MgO layers as well as its concentration θ and also by introducing a metal support below an ultrathin film of the MgO surface. However, performing DFT calculations on the supported clusters can be computationally demanding, especially as one needs to explore the phase space of various possible adsorption sites and structural configurations. One would, therefore, like to know whether one can predict the ground state geometry and/or the charge acquired by the Au clusters from the properties of the doped supports alone. As mentioned in the Introduction, our previously introduced descriptor $\mathscr{D} = \Delta\chi/\Delta\mathscr{R}$ cannot be used to determine which dopant concentration might be optimal in order to achieve a desired charge state and morphology for the adsorbed Au cluster. We, therefore, now look for a descriptor that allows us to also examine the effects of varying concentration θ.

Along these lines, one property of the support that one might consider examining could be the work function of the support.[55,87] One would, in general, expect that the lower the work function, the easier it would be for the support to donate electrons to the adsorbed metal clusters and thus the greater the negative charge acquired by the Au cluster.

FIG. 9. Plot of d, the shortest distance between the Au atom (in the Au nanocluster) and the support, vs $Q(Au_n)$, the charge on the Au cluster, for the Au monomer and dimer at $\theta = 5.55\%$. The red and blue dots show the Au monomer on the donor-doped and acceptor-doped supports, respectively. The red and blue triangles are for the Au dimer on the donor-doped and acceptor-doped supports, respectively. Note the opposing trends for the donor-doped and acceptor-doped systems.

Undoped MgO is an insulator, with the Fermi level falling within the bandgap. However, when the MgO(001) film is doped with donors or acceptors, it becomes electron rich or deficient, respectively, and the position of the Fermi level E_F shifts accordingly. This can be seen from the electronic densities of states plotted in Figs. 10(a)–10(e) for dopant concentration $\theta = 2.78\%$. In these plots, the contributions from different atoms have been projected out and are plotted in different colors. From these graphs, we see that the dopants that we had previously identified[66] as performing "well" (Al, F, Na, and Li) do not introduce significant modifications to the density of states; their main effect is to shift the position of E_F by changing the electron count. As a result, in the case of the donors Al and F, E_F moves up into the bottom of the conduction band,[7,55,61,88,89] whereas for the acceptors Na and Li, E_F moves down into the top of the valence band.[55] However, the dopant that was previously identified[66] as performing "poorly,", viz., N, displays notably different behavior: it introduces new features in the density of states, the sharp peaks due to the N impurity can be seen clearly slightly above the top of the valence band [see Fig. 10(c)], and E_F lies within these states.[90–92] In other words, when the dopant is F, Al, Na, or Li, there is a high degree of hybridization between the dopant states and the host oxide states, but this is not true when the dopant is N. From these graphs, we see that E_F moves progressively to the right in the order Li → Na → N → Al → F, and one would, therefore, expect the work function to decrease in this order. We emphasize again that a dopant that introduces midgap impurity levels shifts the Fermi level to a lesser extent, and this is correlated with the fact that it results in a smaller change in the charge of the deposited nanoparticles (compare Fig. 10 with Fig. 6); this will become clearer further below when we display correlations between the charge on the deposited gold cluster and the work function of the doped support.

Figures 10(f)–10(j) show similar graphs of the projected densities of states for the doped MgO/Mo, again for $\theta = 2.78\%$; note that now E_F always falls within the conduction band, though its position with respect to the conduction band minimum shifts, especially upon doping with the acceptors.

In Fig. 11, we have shown our results for how the work function of the support is changed as a function of the doping concentration θ for (a) MgO(001) and (b) MgO/Mo(001). On these graphs, there is no point corresponding to the undoped Mg(001) surface, as this system is an insulator; however, we see in Fig. 11(b) a green "four-leaf clover" symbol corresponding to the work function of undoped MgO/Mo(001).

The trends observed in Fig. 11(a) are as expected: doping with an electron acceptor (either anionic N or cationic Na/Li) depletes electrons from the support. It, therefore, costs more energy to remove electrons from the surface, and the work function Φ increases. The greater the doping concentration θ, the larger the increase in Φ. For a given value of θ, we find that Φ of the Na-doped and Li-doped MgO systems is larger than that for the N-doped MgO. This suggests that the efficacy of Na and Li as acceptor-type dopants for MgO is greater than that of N because Li and Na make the MgO(001) surface more electron deficient than N. Φ is much lower for the donor-doped MgO surfaces than that for the acceptor-doped MgO surfaces [see Fig. 11(a)], since the donors make MgO(001) electron-rich. The work functions of Al–MgO and F–MgO systems are similar for a given value of θ. Therefore, both the anionic donor F and cationic donor Al perform equally well. We note that these results about the relative efficacy of the different elemental dopants are in agreement with predictions made using our previously introduced descriptor $\mathscr{D} = \Delta\chi/\Delta\mathscr{R}$[66] and also with the conclusions drawn from the densities of states plots shown in Fig. 10.
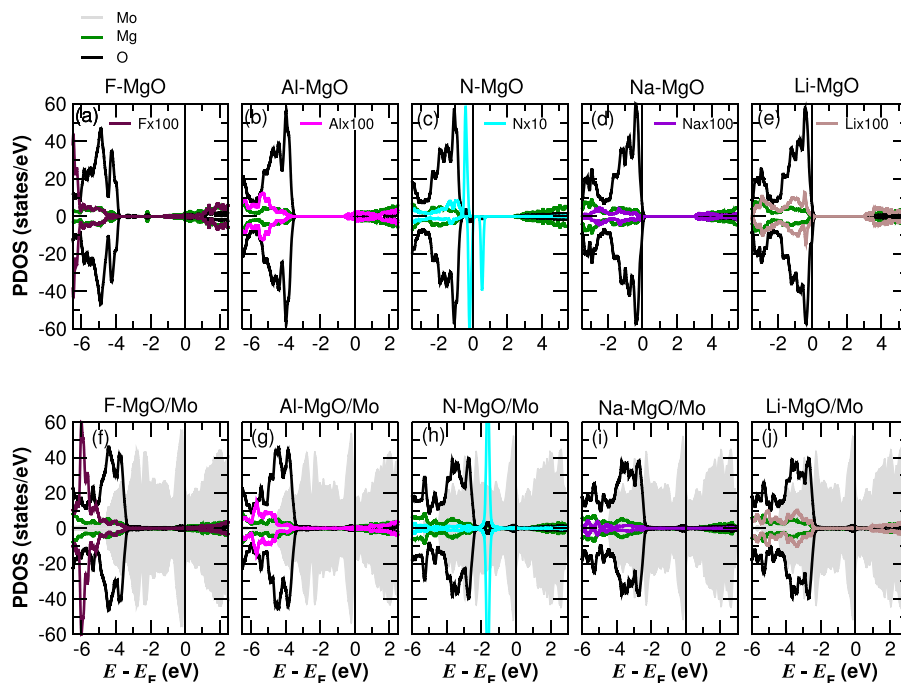

FIG. 10. Plots of the spin polarized projected density of states for MgO(001) doped with $\theta = 2.78\%$ of fluorine, aluminum, nitrogen, sodium, and lithium [(a)–(e)] without and [(f)–(j)] with the Mo substrate. The black, green, maroon, magenta, turquoise, indigo, brown, and gray curves correspond to the contributions from O, Mg, F, Al, N, Na, Li, and Mo atoms, respectively. Note that the contributions from dopant atoms have been magnified for visual clarity.
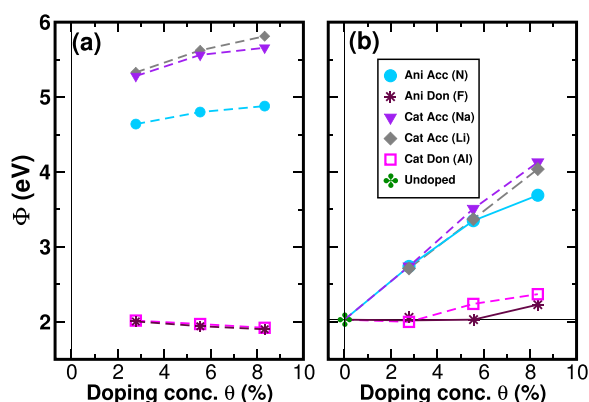
FIG. 11. Work function Φ as a function of doping concentration θ for (a) doped MgO and (b) doped MgO/Mo systems. The green "four-leaf clover" symbol, cyan circles, brown stars, purple triangles, and magenta squares show the undoped, N-doped, F-doped, Na-doped, and Al-doped systems, respectively. The horizontal line in (b) corresponds to Φ for the undoped MgO/Mo, and there is no corresponding line in (a) for undoped MgO as the system is an insulator.

In the case of the doped MgO/Mo(001) systems, the acceptor dopants act as one might expect, with the work function being increased, relative to its value for the undoped case, upon doping. However, the increase in Φ is noticeably less than it was on MgO(001) [compare Figs. 11(a) and 11(b)]; this is because some of the electron depletion due to the presence of the acceptor dopants is offset by electrons flowing into the MgO layers from the Mo layers. Thus, although the net effect is an increase in the work function, the increase is less than it would have been in the absence of the Mo support.

The result that seems initially counter-intuitive is that on MgO/Mo(001), the effect of doping with electron donors is also found to increase the work function, though this effect is small. The source of this increase is rather subtle. Earlier authors have shown that the change in work function at a metal–oxide interface can be viewed as arising from a net dipole moment that can be split up into three contributions: μ_{Comp}, μ_{CT}, and μ_R.[75,93,94] These are the dipole due to electrostatic compression of the free electrons at the interface (see Fig. S1 of the supplementary material), dipole moment due to charge transfer between the metal and oxide (see Fig. S2 of the supplementary material), and the dipole moment due to rumpling (corrugation) of the oxide layer at the interface (see Fig. S3 of the supplementary material), respectively. The dominant contributions are μ_{CT} and μ_R, and these always point in opposite directions. The components of the net dipole moment at the oxide/metal interface are discussed in detail in the supplementary material. Regarding the systems considered here, for the acceptor-doped systems, there is a net transfer of electrons from Mo to MgO and μ_{CT} points downward, whereas for the donor-doped systems, electrons flow from MgO to Mo and μ_{CT} points upward. As far as the rumpling is concerned, in the former case, the corrugation is such that the Mg ions are raised, while the O ions are lowered, while in the latter case, the reverse is true. Accordingly, μ_R points up or down, respectively. For the case of acceptor doping, we find that $|\mu_{CT}| > |\mu_R|$, and thus, all our

intuitive expectations hold. However, for the case of doping with donors, the rumpling is quite significant and $|\mu_R| > |\mu_{CT}|$. For this reason, the change in Φ is opposite what one might expect based on simple arguments.

The work function of any MgO/Mo(001) system depends on the net dipole moment of the corresponding system. A higher value of the dipole moment along the $+\hat{z}$ direction of the combined oxide/metal system makes electron removal from the oxide–metal interface easier. Figure 12 shows the relationship between Φ and the net dipole moment; we see that all the data (for all concentrations of all dopants in MgO/Mo) collapse onto a single straight line. This confirms that changes in the work function are determined by changes in the dipole moment.

Next, we demonstrate that the value of the work function Φ of the support can be used to predict the adsorption geometry and energetics of the deposited Au cluster. In Fig. 13, we have plotted the difference in energy of two competing adsorption geometries, as a function of Φ of the support; the dopant concentration is fixed at 2.78%.

In Fig. 13(a), for the Au monomer, the two competing geometries considered are adsorption at the hollow site and adsorption atop an O atom. The areas of the graph that are shaded yellow and light green correspond to regions where the hollow and atop-O sites are favored, respectively. We see that there is a monotonic and indeed linear relationship between the difference in energy and Φ. Moreover, the data for MgO(001) and MgO/Mo(001) collapse onto a single line.

Similarly, for the Au dimer, we have plotted in Fig. 13(b) the difference in energies between the upright (atop-O) and flat (bonded to two Mg atoms) geometries. Here, yellow and light green shaded regions indicate that the flat and upright geometries are favored, respectively. Once again, we see a monotonic and linear variation of the energy difference with Φ, though in this case, the data corresponding to the doped MgO(001) and doped MgO/Mo(001) supports fall on two different lines. This happens mainly because the flat
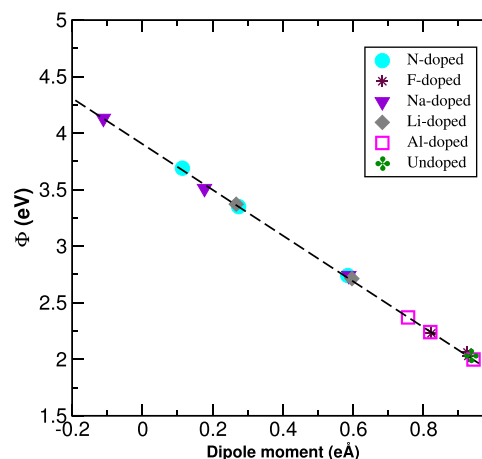

FIG. 12. Work function (Φ) vs dipole moment μ for doped MgO/Mo(001) systems. The cyan circles, maroon stars, purple triangles, gray diamonds, magenta squares, and green "four-leaf clover" symbol show the N-doped, F-doped, Na-doped, Li-doped, Al-doped, and undoped MgO/Mo(001) systems, respectively. Results for all dopant concentrations θ considered have been plotted.
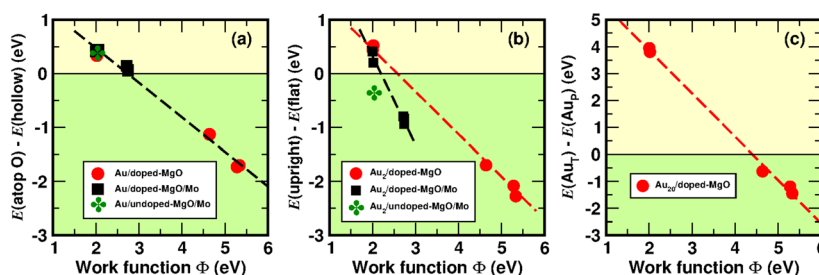
FIG. 13. Performance of Φ as a predictor of adsorption geometry, cluster morphology, and energetics. Energy difference between (a) atop O and hollow sites for Au monomer, (b) the upright (atop O) and flat (bonded to Mg) configurations of Au_2, and (c) the tetrahedral and planar configurations of Au_{20}, all as a function of the work function, Φ. The results are shown at $\theta = 2.78\%$. The red circles and black squares show Au_n on doped MgO and doped MgO/Mo systems, respectively. The green "four-leaf clover" symbol shows undoped MgO/Mo. The yellow regions in (a)–(c) indicate regions where the favored geometry is adsorption of the Au monomer at the hollow site, Au_2 in a flat configuration, and Au_{20} in a planar morphology, respectively, on the doped substrates. In contrast, the light green regions in (a)–(c) indicate regions where the favored geometry is adsorption of the Au monomer atop O, Au_2 in an upright configuration, and Au_{20} in a tetrahedral morphology, respectively.

geometry of the Au dimer on donor-doped MgO(001) is more negatively charged (and therefore more stable) than on donor-doped MgO(001)/Mo due to partial electron transfer from the donor to the Mo substrate in the latter case.

Next, for the Au_{20} cluster, in Fig. 13(c), the difference in E_{ads} between the tetrahedral and planar geometries is plotted as a function of Φ. We see an excellent linear correlation between $E(Au_T)$ – $E(Au_P)$ and Φ. In this graph, the regions shaded yellow and light green indicate that the planar and tetrahedral geometries are favored, respectively. These results indicate that even for the relatively large Au_{20} cluster, the work function Φ of the bare support acts as an excellent descriptor and predictor for the morphology of the deposited cluster. We predict that for $\Phi > 4.47$ eV, the tetrahedral morphology will be favored for the deposited Au_{20} clusters; below this value of work function, the planar morphology will be favored.

Finally, in Fig. 14, we examine whether the work function of the doped support can be used to predict the charge acquired by Au clusters deposited on these supports.

In Fig. 14(a), we see that we obtain a very good linear correlation between the value of Φ for the doped supports, both in the presence and absence of the Mo support, and the value of $Q(Au)$. As in Fig. 13, areas of the graph shaded yellow and light green indicate regions where the favored adsorption is at the hollow site and atop O, respectively. This graph shows, yet again, that it is possible to tune the charge on the Au monomer over a wide range, and it also indicates that it should be possible to predict what this charge will be, by simply computing the work function of the support. We note that in Fig. 14, we have not included data corresponding to MgO/Mo(001) doped with donors; these data do not follow the general trend. This is because of the counter-intuitive trends displayed by Φ for these systems, as has been discussed above.

Figures 14(b)–14(e) contain the corresponding data for the Au dimer, with yellow and light green shading indicating regions where the flat and upright adsorption geometries are favored, respectively. It is clear here that the data fall into two groups, corresponding to the two different adsorption geometries. For $\Phi > 2.03$ eV, the upright geometry is preferred, and it is quite difficult to tune $Q(Au_2)$: a rather large change in Φ results in only a small change in the charge on the Au atoms. However, for $\Phi < 2.03$ eV, the flat geometry becomes favored, and even small changes in Φ have a huge effect on $Q(Au_2)$. Figures 14(c)–14(e) display zoomed-in regions of

the data in Fig. 14(b), enabling one to compare the effects of cationic and anionic dopants.

Similar data for the 20-atom cluster are plotted in Fig. 14(f), where we see that we obtain a linear correlation between $Q(Au_{20})$
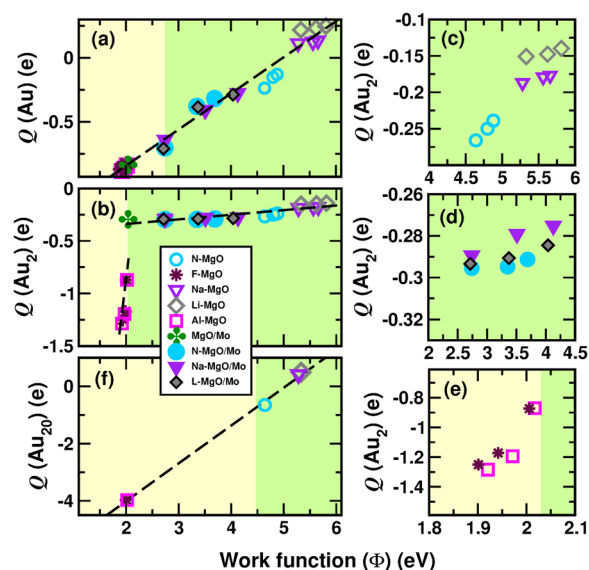

FIG. 14. Performance of Φ as a predictor of the charge acquired by the deposited cluster. Dependence of charge Q gained by (a) Au monomer, [(b)–(e)] Au dimer, and (f) Au_{20} on the work function, Φ, of the support. Zoomed-in views of $Q(Au_2)$ vs Φ plots for Au_2 on (c) N-doped and Na-doped MgO, (d) N-doped and Na-doped MgO/Mo, and (e) F-doped and Al-doped MgO. The cyan circles, maroon stars, purple triangles, and magenta squares show the Au monomer or dimer on the N-doped, F-doped, Na-doped and Al-doped MgO systems, respectively. Solid symbols are used for the doped MgO/Mo systems with the same color conventions as for the doped MgO systems. The green "four-leaf clover" symbol shows undoped MgO/Mo. The yellow regions in (a), (b), and (f) indicate a favored geometry for adsorption of the Au monomer at the hollow site, Au_2 in a flat (bonded to Mg) configuration, and Au_{20} in a planar geometry, respectively, on the doped substrates. The light green regions in (a), (b), and (f), on the other hand, indicate a favored geometry for adsorption of the Au monomer atop O, Au_2 in an upright (bonded to O) configuration, and Au_{20} in a tetrahedral geometry, respectively, on the doped substrates.

and Φ. Note that due to computational constraints, in this case, we have restricted ourselves to considering changes in Φ that arise only from changes in the dopant element, with θ fixed at 2.78%. As in Fig. 13(c), the yellow and light green shaded regions indicate the regions where the favored morphology for Au_{20} deposited on the doped support is planar and tetrahedral, respectively. The boundary between the yellow and green shaded regions is obtained from the value of Φ corresponding to $E(Au_T)$ − $E(Au_P) = 0$ in Fig. 13(c). This graph underlines that it is possible to tune the charge of Au_{20} over a wide range by changing the nature of the dopant; intermediate values of charge, as well as a wider range, can be obtained by varying the dopant concentration θ, as was done for the cases of the Au monomer and dimer above.

V. SUMMARY AND CONCLUSIONS

In summary, we have used *ab initio* density functional theory calculations to investigate the possibility of tuning the charge of Au nanoparticles by appropriately doping the oxide support that they are placed on, with aliovalent cations or anions. We find that the cationic acceptors Li and Na (unlike the anionic acceptor N) can make the Au monomer, as well as the significantly larger Au_{20} cluster, positively charged and are thus better dopants. However, the cationic donor Al and the anionic donor F perform equally well in making the clusters negatively charged. The performance of the dopants in this respect can be traced back to features in the densities of states: dopants that introduce impurity levels that fall within the gap of the oxide support do not result in large changes in support work function and hence do not significantly alter the charge transferred to the deposited cluster. In contrast, dopants whose states lie well within the valence and conduction bands of the oxide support (i.e., there is a large degree of hybridization between the dopant states and the oxide states) result in large changes in work function and hence large changes in charge transfer.

For the range of doping concentrations studied here, we were able to vary the charge $Q(Au)$ from $-0.88e$ to $+0.14e$. For the Au dimer, we were able to tune the charge $Q(Au_2)$ between $-1.28e$ and $-0.18e$, and in no case did the Au dimer become positively charged. These changes in the charge state could be correlated with changes in adsorption geometry: when the Au atoms became more negatively charged, the Au monomer switched its adsorption site from atop an O atom to the hollow site on the surface, while the Au dimer transitioned from an upright to flat geometry. Similar results were obtained when the support was an ultrathin MgO slab placed on a Mo support, though now the range of values over which the charge could be tuned was reduced: $-0.88e < Q(Au) < -0.27e$ and $-1.19e < Q(Au_2) < -0.27e$. We find that if one is doping the oxide support, the only benefit of introducing the Mo substrate in addition is that one gains the ability to have finer control over the negative charge acquired by the Au clusters at small donor doping concentrations.

Concomitant with the changes in the charge of the Au cluster, there are changes in its magnetic moment, which varies between 0 μ_B and 0.75 μ_B for the monomer and between 0 μ_B and 0.77 μ_B for the dimer.

For the Au_{20} cluster, we restricted ourselves to studying $\theta = 2.78\%$ for the doped Mg0(001) supports. By varying the dopant species, we were able to vary the charge $Q(Au_{20})$ from $-3.97e$ to $+0.49e$. As the cluster became more negatively charged, it transitioned from a three-dimensional tetrahedral geometry to a two-dimensional planar geometry. The Au_{20} cluster remained non-magnetic in all cases considered by us.

Importantly, we find that the work function Φ of the doped support can serve as a descriptor for both the adsorption geometry and the charge of the deposited Au cluster (with the notable exception of the case when the oxide is donor-doped as well as supported by a metal). As the work function increases, one sees that the charge acquired by the deposited Au cluster becomes monotonically less negative (more positive), and there is a transition from a wetting to a non-wetting geometry (for the monomer, this transition is from a position adsorbed at a hollow site to one atop O).

As calculating the work function of the doped support is computationally much cheaper than performing calculations on deposited clusters, using the work function as a descriptor can save considerable time and effort in predicting cluster geometries and charges. We note that these geometries and charge states, in turn, play a determining role in the performance of these systems as nanocatalysts; it is well known that for different reactions with Au catalysts, different charges on the Au catalysts are to be preferred. In this context, we point out that our success in charging the Au monomer and Au_{20} cluster positively by using the Na- or Li-doped MgO as a support is of considerable interest, given the high electronegativity of Au, and the consequent challenges posed in getting Au clusters to be positively charged.

Compared to our previously introduced descriptor $\mathscr{D} = \Delta\chi/\Delta\mathscr{R}$,[66] the computation of the work function Φ is slightly more expensive. However, it has the considerable advantage that it allows one to describe the effects of changing the dopant concentration θ.

SUPPLEMENTARY MATERIAL

See the supplementary material for discussion of the various contributions to the net dipole moment at the interface of an oxide/metal system and our corresponding results.

ACKNOWLEDGMENTS

REFERENCES

[1] M. Haruta and M. Daté, Appl. Catal., A **222**, 427 (2001).
[2] M. Z. Herrera, J. Aizpurua, A. K. Kazansky, and A. G. Borisov, Langmuir **32**, 2829 (2016).
[3] H. Chugh, D. Sood, I. Chandra, V. Tomar, G. Dhawan, and R. Chandra, Artif. Cells, Nanomed., Biotechnol. **46**, 1210 (2018).
[4] J. B. Vines, J.-H. Yoon, N.-E. Ryu, D.-J. Lim, and H. Park, Front. Chem. **7**, 167 (2019).
[5] P. Frondelius, H. Häkkinen, and K. Honkala, New J. Phys. **9**, 339 (2007).

[6]C. Zhang, A. Michaelides, D. A. King, and S. J. Jenkins, J. Am. Chem. Soc. **132**, 2175 (2010).

[7]N. Mammen, S. Narasimhan, and S. de Gironcoli, J. Am. Chem. Soc. **133**, 2801 (2011).

[8]L. Giordano, M. Baistrocchi, and G. Pacchioni, Phys. Rev. B **72**, 115403 (2005).

[9]M. Gao, A. Lyalin, and T. Taketsugu, Catalysts **1**, 18 (2011).

[10]M. Zhu, C. M. Aikens, M. P. Hendrich, R. Gupta, H. Qian, G. C. Schatz, and R. Jin, J. Am. Chem. Soc. **131**, 2490 (2009).

[11]S. Antonello, N. V. Perera, M. Ruzzi, J. A. Gascón, and F. Maran, J. Am. Chem. Soc. **135**, 15585 (2013).

[12]H. Choi, W. T. Chen, and P. V. Kamat, ACS Nano **6**, 4418 (2012).

[13]A. Prestianni, A. Martorana, F. Labat, I. Ciofini, and C. Adamo, J. Phys. Chem. B **110**, 12240 (2006).

[14]N. Lopez and J. K. Nørskov, J. Am. Chem. Soc. **124**, 11262 (2002).

[15]A. Corma and H. Garcia, Chem. Soc. Rev. **37**, 2096 (2008).

[16]X. Wu, L. Senapati, S. K. Nayak, A. Selloni, and M. Hajaligol, J. Chem. Phys. **117**, 4010 (2002).

[17]Z.-P. Liu, P. Hu, and Ali Alavi, J. Am. Chem. Soc. **124**, 14770 (2002).

[18]A. Lyalin and T. Taketsugu, J. Phys. Chem. C **114**, 2484 (2010).

[19]G.-J. Kang, Z.-X. Chen, Z. Li, and X. He, J. Chem. Phys. **130**, 034701 (2009).

[20]Y. Jv, B. Li, and R. Cao, Chem. Commun. **46**, 8017 (2010).

[21]J. Graciani, A. Nambu, J. Evans, J. A. Rodriguez, and J. F. Sanz, J. Am. Chem. Soc. **130**, 12056 (2008).

[22]B. Yoon, H. Häkkinen, and U. Landman, J. Phys. Chem. A **107**, 4066 (2003).

[23]A. Lyalin, K. Uosaki, and T. Taketsugu, Electrocatalysis **9**, 182 (2018).

[24]J. P. H. Li, Z. Liu, H. Wu, and Y. Yang, Catal. Today **307**, 84 (2018).

[25]J. Good, P. N. Duchesne, P. Zhang, W. Koshut, M. Zhou, and R. Jin, Catal. Today **280**, 239 (2017).

[26]W. Y. Hernández, F. Aliç, S. Navarro-Jaen, M. A. Centeno, P. Vermeir, P. Van Der Voort, and A. Verberckmoes, J. Mater. Sci. **52**, 4727 (2017).

[27]C. Zhang, B. Yoon, and U. Landman, J. Am. Chem. Soc. **129**, 2228–2229 (2007).

[28]J. Elliott, J. Duay, O. Simoska, J. B. Shear, and K. J. Stevenson, Am. J. Anal. Chem. **89**, 1267 (2017).

[29]E. V. Milsom, J. Novak, M. Oyama, and F. Marken, Electrochem. Commun. **9**, 436 (2007).

[30]L. A. Calzada, S. E. Collins, C. W. Han, V. Ortalan, and R. Zanella, Appl. Catal. B: Environ. **207**, 79 (2017).

[31]E. E. Stangland, K. B. Stavens, R. P. Andres, and W. N. Delgass, J. Catal. **191**, 332 (2000).

[32]B. S. Uphade, S. Tsubota, T. Hayashi, and M. Haruta, Chem. Lett. **27**, 1277 (1998).

[33]L. Rout, A. Kumar, R. S. Dhaka, G. N. Reddy, S. Giri, and P. Dash, Appl. Catal. A: General **538**, 107 (2017).

[34]L. Ma, K. Laasonen, and J. Akola, J. Phys. Chem. C **121**, 10876 (2008).

[35]C. Gao, Y. Hu, M. Wang, M. Chi, and Y. Yin, J. Am. Chem. Soc. **136**, 7474 (2014).

[36]L. Zhang, A. Wang, J. T. Miller, X. Liu, X. Yang, W. Wang, L. Li, Y. Huang, C.-Y. Mou, and T. Zhang, ACS Catal. **4**, 1546 (2014).

[37]T. Joseph, K. Vijay Kumar, A. V. Ramaswamy, and S. B. Halligudi, Catal. Commun. **8**, 629 (2007).

[38]S. Dong, Y. Zhang, X. Zhang, J. Mao, and Z. Yang, Appl. Surf. Sci. **426**, 554 (2017).

[39]X. Lin, B. Yang, H.-M. Benia, P. Myrach, M. Yulikov, A. Aumer, M. A. Brown, M. Sterrer, O. Bondarchuk, E. Kieseritzky, J. Rocker, T. Risse, H.-J. Gao, N. Nilius, and H.-J. Freund, J. Am. Chem. Soc. **132**, 7745 (2010).

[40]Y.- G. Wang, D. Mei, V. A. Glezakou, J. Li, and R. Rousseau, Nat. Commun. **6**, 6511 (2015).

[41]J.-C. Liu, Y.-G. Wang, and J. Li, J. Am. Chem. Soc. **139**, 6190 (2017).

[42]M. M. Schubert, S. Hackenberg, A. C. van Veen, M. Muhler, V. Plzak, and R. J. Behm, J. Catal. **197**, 113 (2001).

[43]A. R. Puigdollers, P. Schlexer, and G. Pacchioni, J. Phys. Chem. C **119**, 15381 (2015).

[44]T. Lozano and R. B. Rankin, Front. Chem. **7**, 610 (2019).

[45]A. S. Crampton, M. D. Rötzer, U. Landman, and U. Heiz, ACS Catal. **7**, 6738 (2017).

[46]L. A. Kappers, R. L. Kroes, and E. B. Hensley, Phys. Rev. B **1**, 4151 (1970).

[47]B. Yoon, H. Häkkinen, U. Landman, A. S. Wörz, J.-M. Antonietti, S. Abbet, K. Judai, and U. Heiz, Science **307**, 403 (2005).

[48]A. Del Vitto, G. Pacchioni, F. Delbecq, and P. Sautet, J. Phys. Chem. B **109**, 8040 (2005).

[49]Z. Yang, R. Wu, Q. Zhang, and D. W. Goodman, Phys. Rev. B **65**, 155407 (2002).

[50]P. Frondelius, H. Häkkinen, and K. Honkala, Phys. Rev. B **76**, 073406 (2007).

[51]K. Honkala and H. Häkkinen, J. Phys. Chem. C **111**, 4319 (2007).

[52]V. Simic-Milosevic, M. Heyde, N. Nilius, T. König, H.-P. Rust, M. Sterrer, T. Risse, H.-J. Freund, L. Giordano, and G. Pacchioni, J. Am. Chem. Soc. **130**, 7814 (2008).

[53]J. Nevalaita, H. Häkkinen, and K. Honkala, J. Phys. Chem. C **121**, 10824 (2017).

[54]T. Risse, S. Shaikhutdinov, N. Nilius, M. Sterrer, and H.-J. Freund, Acc. Chem. Res. **41**, 949 (2008).

[55]S. Prada, L. Giordano, and G. Pacchioni, J. Phys. Chem. C **116**, 5781 (2012).

[56]F. Stavale, X. Shao, N. Nilius, H.-J. Freund, S. Prada, L. Giordano, and G. Pacchioni, J. Am. Chem. Soc. **134**, 11380 (2012).

[57]S. Prada, L. Giordano, and G. Pacchioni, J. Am. Chem. Soc. **117**, 9943 (2013).

[58]B. Yoon and U. Landman, Phys. Rev. Lett. **100**, 056102 (2008).

[59]N. Mammen and S. Narasimhan, J. Chem. Phys. **149**, 174701 (2018).

[60]Y.-G. Wang, Y. Yoon, V.-A. Glezakou, J. Li, and R. Rousseau, J. Am. Chem. Soc. **135**, 10673 (2013).

[61]N. Mammen, S. de Gironcoli, and S. Narasimhan, J. Chem. Phys. **143**, 144307 (2015).

[62]S. Liang, C. Hao, and Y. Shi, ChemCatChem **7**, 2559–2567 (2015).

[63]B. Qiao, J.-X. Liang, A. Wang, C.-Q. Xu, J. Li, T. Zhang, and J. J. Liu, Nano Res. **8**, 2913–2924 (2015).

[64]D. Ricci, A. Bongiorno, G. Pacchioni, and U. Landman, Phys. Rev. Lett. **97**, 036106–036110 (2006).

[65]L. Molina and B. Hammer, J. Catal. **233**, 399–404 (2005).

[66]S. Ghosh, N. Mammen, and S. Narasimhan, J. Phys. Chem. C **123**, 19794 (2019).

[67]L. M. Ghiringhelli, J. Vybiral, S. V. Levchenko, C. Draxl, and M. Scheffler, Phys. Rev. Lett. **114**, 105503 (2015).

[68]L. Himanen, M. O. Jäger, E. V. Morooka, F. Federici Canova, Y. S. Ranawat, D. Z. Gao, P. Rinke, and A. S. Foster, Comput. Phys. Commun. **247**, 106949 (2020).

[69]C. Klanner, D. Farrusseng, L. Baumes, M. Lengliz, C. Mirodatos, and F. Schüth, Angew. Chem., Int. Ed. **43**, 5347 (2004).

[70]K. T. Butler, J. M. Frost, J. M. Skelton, K. L. Svane, and A. Walsh, Chem. Soc. Rev. **45**, 6138 (2016).

[71]S. Baroni, A. dal Corso, S. de Gironcoli, P. Giannozzi, C. Cavazzoni, G. Ballabio, S. Scandolo, G. Chiarotti, P. Focher, A. Pasquarello, K. Laasonen, A. Trave, R. Car, and N. Marzari, J. Phys. Condens. Matter **21**, 395502 (2009).

[72]W. Kohn and L. J. Sham, Phys. Rev. **140**, A1133 (1965).

[73]D. Vanderbilt, Phys. Rev. B **41**, 7892 (1990).

[74]J. P. Perdew and Y. Wang, Phys. Rev. B **46**, 12947 (1992).

[75]S. Ling, M. B. Watkins, and A. L. Shluger, Phys. Chem. Chem. Phys. **15**, 19615 (2013).

[76]T. C. Leung, C. L. Kao, W. S. Su, Y. J. Feng, and C. T. Chan, Phys. Rev. B **68**, 195408 (2003).

[77]H. J. Monkhorst and J. D. Pack, Phys. Rev. B **13**, 5188 (1976).

[78]N. Marzari, D. Vanderbilt, A. De Vita, and M. C. Payne, Phys. Rev. Lett. **82**, 3296 (1999).

[79]R. P. Feynman, Phys. Rev. **56**, 340 (1939).

[80]A. J. Logsdail, D. O. Scanlon, C. R. A. Catlow, and A. A. Sokol, Phys. Rev. B **90**, 155106 (2014).

[81]N. E. Singh-Miller and N. Marzari, Phys. Rev. B **80**, 235407 (2009).

[82]R. F. W. Bader, *Atoms in Molecules: A Quantum Theory* (Oxford University Press, New York, 1990).

[83]W. Tang, E. Sanville, and G. Henkelman, J. Phys. Condens. Matter **21**, 084204 (2009).

[84] S. Sicolo, L. Giordano, and G. Pacchioni, J. Phys. Chem. C **113**, 16694 (2009).

[85] J. Li, X. Li, H.-J. Zhai, and L.-S. Wang, Science **299**, 864–867 (2003).

[86] P. Schlexer, A. Ruiz Puigdollers, and G. Pacchioni, Phys. Chem. Chem. Phys. **17**, 22342 (2015).

[87] L. Giordano, F. Cinquini, and G. Pacchioni, Phys. Rev. B **73**, 045414 (2006).

[88] R. Saha, S. Revoju, V. I. Hegde, U. V. Waghmare, A. Sundaresan, and C. N. R. Rao, Chem. Phys. Chem. **14**, 2672–2677 (2013).

[89] J. Xu, S. Huang, and Z. Wang, Solid State Commun. **149**, 527–531 (2009).

[90] P. Mavropoulous, M. Lezaic, and S. Blugel, Phys. Rev. B **80**, 184403 (2009).

[91] Z. Zhu, B. Bian, and H. Shi, J. Semicond. **36**, 102003 (2015).

[92] Y. Li, K. Ding, B. Cheng, Y. Zhang, and Y. Lu, Phys. Chem. Chem. Phys. **17**, 5613–5623 (2015).

[93] J. Goniakowski and C. Noguera, Phys. Rev. B **79**, 155433 (2009).

[94] S. Prada, U. Martinez, and G. Pacchioni, Phys. Rev. B **78**, 235423 (2008).